JEMMME (Journal of Energy, Mechanical, Material, and Manufacturing Engineering)
Vol. 9, No. 2, 2024

ISSN 2541-6332 | e-ISSN 2548-4281
Journal homepage: http://ejournal.umm.ac.id/index.php/JEMMME

Modeling and simulation of magnet-coil arrays for vibrational energy harvesting in agricultural electric vehicles

Mbanwei Divine Kobbi[a, b]*, Njimboh Henry Alombah[b], Ngwa Martin Ngwabie[a]
[a]Department of Agricultural and Environmental Engineering, College of Technology, The University of Bamenda, Bambili, Cameroon
[b]Department of Electrical and Electronic Engineering, College of Technology, The University of Bamenda, Bambili, Cameroon
*e-mail: divine.kobbi@uniba.cm

Abstract

Electric vehicles have advantages such as reduced maintenance and fuel costs compared to internal combustion engines. However, their limited driving range still hinders their widespread adoption compared to internal combustion engines. Harvesting wasted energies through vibrations in electric vehicles is a good approach to complement the energy of their batteries. Space constraints in electric vehicles require devices with high power output per unit volume. This study aimed to design a novel vibration energy harvesting using the geometrical model for electric vehicles. Different configurations and their performance in maximum flux linkage, electromagnetic coupling coefficient, induced voltage, and generated power were investigated. The modeling, excitement, and analysis were conducted using ANSYS Maxwell software with four configurations under similar conditions. These were the Halbach array with three magnets, one coil, and flat back shield; the Halbach array with three magnets and one coil with a stepped back shield; the double magnet array with two magnets, one coil, and flat back shield; and the fourth one was a double magnet array with two magnets, one coil and stepped back shield. The MATLAB Simulink software was used to obtain further results and power output analysis. The results of the analysis show that the Halbach array with three magnets, one coil, and a stepped-back shield is the best configuration for harvesting energy from vibrations, producing an electromagnetic coupling coefficient of up to 110 Wb/m, a voltage of up to 36 V, and generated power density of 0.13 W/cm. A reasonable increase in output using less volume was obtained compared to the other studies. The energy harvested will be applied in future studies to extend the range of agricultural electric vehicles, reducing farmers' income spent on fuel and maintenance.

Keywords*: agricultural transportation; electric vehicles; electromagnetic vibration energy harvester volume; electromagnetic coupling coefficient; Halbach magnet arrays*

1. INTRODUCTION

The agricultural sector is vital to global food security, but it faces challenges in transportation costs due to its significant impact on farmers' income (1, 2). Thus, the effects of transportation costs on farmers' income must be minimized (3). Electric vehicles (EVs) offer a promising solution for agricultural transportation. EVs have numerous advantages such as reduced maintenance and low costs for fuel. Electric motors have fewer moving parts than internal combustion engine (ICE) vehicles, resulting in lower maintenance costs and less downtime for farmers. Moreover, concerning fuel efficiency and cost savings, EVs eliminate reliance on fossil fuels, significantly reducing operational costs associated with fuel purchases. EVs are also environmentally friendly producing zero greenhouse gas emissions, contributing to cleaner air and a more sustainable agricultural ecosystem (4).

However, a key drawback to the widespread adoption of EVs in agriculture is their limited range compared to ICE vehicles (5). This limitation can be particularly troublesome for farmers who must transport farm inputs and outputs through isolated areas without charging stations for EV batteries with ranges of only 150 to 200km (6). To address this challenge, research focuses on innovative solutions that can extend the range of electric vehicles through energy harvesting (7). This will facilitate their adoption in agricultural transportation. One such promising area of research is vibration energy harvesting (VEH).

The VEH technology has the potential to enhance agricultural transportation by capturing the wasted energies from vehicle vibrations during operation (8). Furthermore, this captured energy can be converted into electrical energy, and more can be used to recharge electric vehicles' batteries. This effectively extends their range or maximizes the efficiency of the battery supply.

Studies have shown that the configuration of magnets and coils within a VEH system impacts the amount of energy harvested (9-11). Among various configurations, those employing three magnets with a Halbach magnet-coil arrangement and two magnets with a coil arrangement have demonstrated higher performance (12, 13). These configurations optimize the magnetic field for improved flux linkage with the coil, a crucial factor in determining the amount of energy captured.

While existing studies highlight the effectiveness of these magnet coil configurations, further research is needed to develop better-performing vibration energy harvesters. This study aimed to produce a more productive geometrical configuration of a VEH and study its effect on flux linkage, power, and voltage outputs using a smaller volume since space requirement is a constraint in the electric vehicle power system. The energy harvested will be used to extend the driving range of agricultural electric vehicles in future studies.

The current research delved into the effects of geometrical configuration on the performance of the VEH using the Halbach three magnets-coil array and the double magnet-coil array. Various geometrical configurations' performances were investigated by implementing the modeling and simulation techniques. It was mainly to identify the optimal configuration that maximizes flux linkage with the coil, leading to the highest possible power and voltage output from the VEH system.

2. METHODS

The modeling and simulation techniques were employed in this study to evaluate the performance of various magnet-coil configurations containing adjusted back shields. By utilizing specialized software and design tools (ANSYS Maxwell, Simplorer, and MATLAB), virtual models of the VEH system were created and their operation was simulated under similar excitation conditions. The simulations permitted the analysis of the impact of different configurations on key performance metrics such as power output, voltage generation, and overall efficiency.

2.1 The electromagnetic vibration energy harvester

There are principally three types of vibration energy harvesters. They are the piezoelectric, electrostatic, and electromagnetic vibration energy harvesters (14). Piezoelectric harvesters rely on the piezoelectric effect, where certain materials like lead zirconate titanate (PZT) generate a voltage when mechanically stressed (15, 16). Electromagnetic VEH designs utilize a coil and magnet arrangement. Vibrations cause relative movement between the magnet and coil, inducing a current in the coil according to Faraday's Law of electromagnetic induction (9, 17). Electrostatic Vibration Energy harvester designs exploit the principle of varying capacitance between two plates. Vibrations cause a change in the distance between the plates, altering the capacitance and generating a voltage across them (18, 19).

While all technologies have their place, in designing and modeling a VEH for an agricultural tricycle, an electromagnetic harvester is generally the most recommended option for several reasons. It is such as scalability since their designs can be tailored to fit the size and weight constraints of the tricycle. Concerning tunable resonance, one can optimize the harvester to resonate at the dominant vibration frequency experienced by the tricycle while traveling. Moreover, they have relatively high power output compared to electrostatic harvesters. Electromagnetic designs can generate enough power to contribute

meaningfully to the tricycle battery. Electromagnetic harvesters have lower maintenance; their simpler design with fewer moving parts translates to lower maintenance requirements. They have a higher efficiency, simple configuration, and cost (20, 21). The electromagnetic vibration energy harvester (EVEH) model was thus used for this research.

The electromagnetic vibration energy harvester is a device that converts the vibrations of their environment into electrical energy (22, 23). They have two key components. That is the mechanical and electrical parts. The description of the various parts and operating principle is compiled from studies in (17, 19).

The mechanical part constitutes the magnet. This is an important component of the powerhouse of the harvester, a permanent magnet made of the neodymium iron boron (NdFeB) material. The magnet creates a static magnetic field within the harvester. The copper coil which is a tightly wound wire is wrapped around in a cylindrical manner. The coil sits within the magnetic field generated by the magnet. Linked to the magnet is usually a seismic mass. The seismic mass is a weight attached to a spring or other flexible structure. The seismic mass is designed to resonate at the desired vibration frequency. The mechanical part is completed with the spring. This component provides mechanical support for the seismic mass and allows it to move freely in response to vibrations.

For effective performance, additional external circuitry is present, and is used for impedance matching (ensuring efficient power transfer) and voltage regulation (providing a stable output voltage). The core principle behind the EVEH operation is Faraday's Law of electromagnetic induction (24-26).

There are generally two types of coil magnet architectures used in the EVEH. That is the magnet in-line coil architecture and the magnet across coil architecture (9). In the architecture of a magnet in-line coil, the permanent magnet and the coil are positioned along the same axis. The magnet sits inside the coil, with the magnetic field running through the center of the coil. This arrangement is accompanied by a back iron plate or the shield is placed behind the magnet. As the seismic mass vibrates, the magnet moves slightly within the coil. This movement changes the magnetic flux passing through the coil, inducing a current according to Faraday's Law. The back iron plate helps to channel and concentrate the magnetic field, further enhancing the efficiency of flux linkage with the coil. In the magnet across-coil configuration, the permanent magnet is positioned perpendicular to the axis of the coil. The magnet sits on one side of the coil, with its magnetic field passing through the width of the coil. Vibrations cause the seismic mass to move, altering the distance between the magnet and the coil. This change in distance results in a variation of the magnetic flux passing through the coil, inducing a current. However, the magnet in-line architecture is the most widely used mechanism for the EVEH while the magnet across configuration is under study for application (13). The magnet in-line coil in Figure 1 was the architecture chosen for this research work.

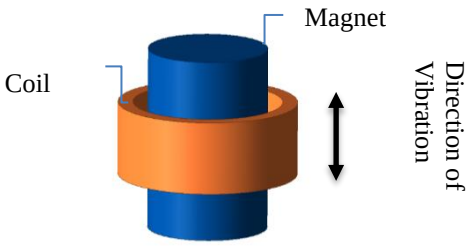

Figure 1. Architectural array of the magnet in-line coil structure showing the placement of the magnet in line with the magnet

2.2 The Halbach magnet array

The EVEH relies on the efficient interaction between magnets and coils to convert vibrations into electricity. The Halbach array, a specific arrangement of permanent magnets, offers a unique approach to enhance this interaction and boost the performance of EVEH designs. Unlike the standard configuration that constitutes a row of permanent magnets placed side-by-side, all magnetized in the same direction, the Halbach array takes

a different approach. It involves alternating the magnetization direction of adjacent magnets in a specific pattern. This seemingly simple arrangement creates a remarkable effect. On one side of the array, the magnetic fields of the alternating magnets reinforce each other, creating a significantly stronger magnetic field than a standard arrangement. Conversely, the alternating fields partially cancel each other out on the other side of the array, resulting in a drastically weaker magnetic field. This unique property of the Halbach array offers distinct advantages for the EVEH applications (27, 28).

The Halbach array is implemented into the EVEH design by placing it on one side of the coil, with a strong magnetic field directed towards the coil. The weaker magnetic field on the opposite side minimizes interference with other components in the harvester. There are primarily two types of Halbach arrays. That is the circular Halbach array and the linear Halbach array (29). The linear Halbach array was chosen for this research work based on the structural requirements and suitability for the design. The simulations were done using the method of finite element analysis which is an important tool in design and simulations (30).

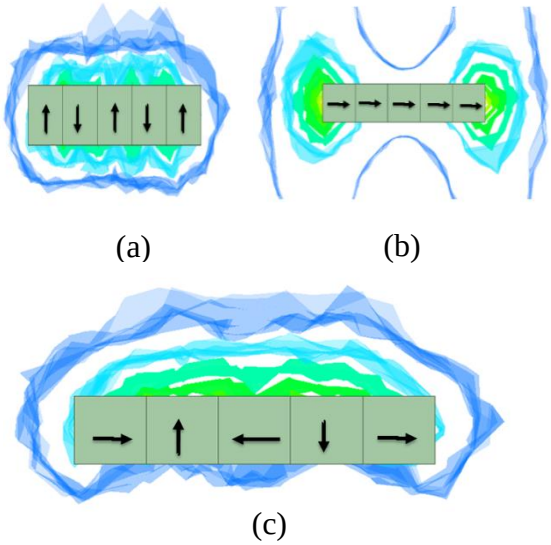

Figure 2. Schematic representation of a linear magnet array showing the (a) alternating magnet, (b) head-to-tail magnet, and (c) Halbach magnet arrays with concentrated fields on one side of the magnet array

Figure 2 shows the normal arrangement and the linear Halbach arrangement of magnets. The magnets and their orientation are shown using arrows while the generated resultant combined magnetic field flux lines are shown in color around the magnet arrays. The models were done using the Finite Element Method Magnetics (FEMM) which is software for solving electromagnetic problems on 2D planar and axisymmetric domains (31). The software used here is ANSYS Maxwell R2023. The program addresses both linear and nonlinear magnetostatic and transient problems (32). It is seen that the magnetic flux is more concentrated in the Halbach array in Figure 2 (c) unlike the normal arrays shown in Figures 2 (a) and (b). As mentioned earlier, this magnetic field concentration is useful in harvesting more energy from the EVEH as the coil will be linked to more flux.

2.3 Modelling of the electromagnetic vibration energy harvester

The VEH mechanical model describes the harvester's movement due to vibrations. It's typically represented as a single-degree-of-freedom second-order mass-spring-damper system, as shown in Figure 3.

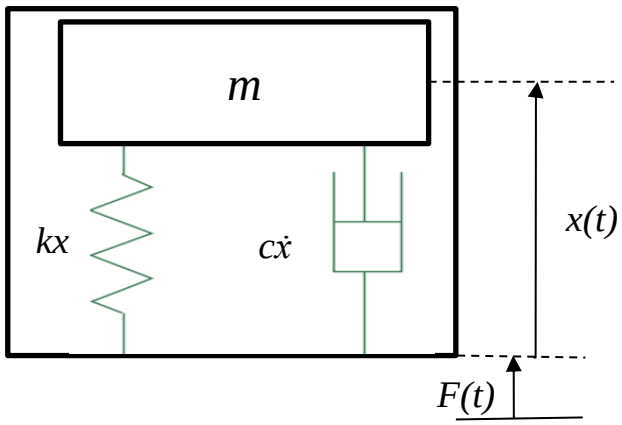

Figure 3. Mechanical model of the EVEH using a mass spring damper system

The ANSYS Simplorer mechanical analogous and electrical domains of the EVEH are shown in Figure 4.

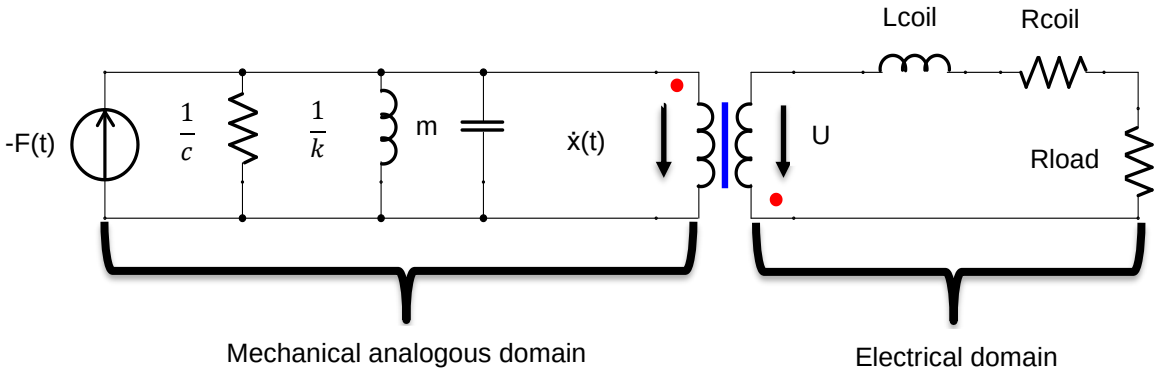

Figure 4. An ANSYS Simplorer developed a model showing the mechanical, and electrical domains and components of the EVEH

Mathematically, the mechanical system of the EVEH is represented in equation (1).

$$m\ddot{x}(t) + c\dot{x}(t) + kx(t) = -F(t) \quad (1)$$

Where *m* is the mass of the vibrating magnet (kg), *c* is the damping coefficient representing energy dissipation (due to friction), *k* is the spring constant representing the stiffness of the structure, *x(t)* is the displacement of the mass relative to its rest position (m), $\dot{x}(t)$ is the velocity of the mass (m/s), $\ddot{x}(t)$ is the acceleration of the mass (m/s^2), *F(t)* is the external force or excitation due to vibration (N), and *t* is the time of vibration (s).

The differential equations governing the transducer are derived from equations (2) and (3). Equation (1) is the equation of an unloaded oscillator. When loaded with an electrical load, an extra term is added to (1) as the induced current flows. The back action of the induced current introduces a constant *K*, which is the electromagnetic coupling coefficient (transduction factor) as shown in equation (2) (33, 34).

$$m\ddot{x}(t) + c\dot{x}(t) + kx(t) + Ki(t) = -F(t) \quad (2)$$
$$U(t) = K\dot{x}(t) = (Rcoil + Rload)i(t) + Lcoil\,.\,i(t) \quad (3)$$

Equation (3) represents the electrical model of the EVEH. The electrical model describes the conversion of mechanical motion into electrical energy. *Rcoil, Rload,* and *Lcoil* represent the coil resistance, load, and inductance of the coil respectively. The induced voltage *U(t)*, is derived from Faraday's law of electromagnetic induction as follows:

$$U(t) = -N\frac{d\varphi}{dt} = -N\frac{d\varphi}{dx}\dot{x}(t) = K\dot{x}(t) \quad (4)$$

Where *N* is the number of turns of the coil while *φ* represents the flux of one coil turn. *K* depends on the geometry of the coil and the magnetic configuration or circuit (35). Equation (4) shows that the energy harvested or induced voltage depends on the number of turns including the change in position of the magnet relative to the coil and the speed of the magnet. The term $N\frac{d\varphi}{dx}$ represents the electromagnetic coupling coefficient *(K)* while $\dot{x}(t)$ represents the speed of the magnet as the seismic mass of the VEH vibrates. Thus, *K* depends on the number of turns of the coil and the flux linkage to the coil or change in flux which are quantities that depend on the geometry of the VEH. Since the generated power depends on *K* which in turn depends on the geometry, the geometry alteration significantly affects the power generated.

At low frequencies, the coil inductance *(Lcoil)* is zero. Solving for the current *(i(t))* in equation (3) and substituting in (2) shows an additional electrical coefficient of damping (Ce), which results from the back action of the induced current on the harvester's mechanical part.

$$i(t) = \frac{K\dot{x}(t)}{Rcoil+Rload} \quad (5)$$

The expression for *Ce* is shown in equation (6) and the current in (5).

$$Ce = \frac{K^2}{Rcoil+Rload} \quad (6)$$

Following the theory of maximum power transfer on the application of impedance matching, maximum power is transferred to the load when the optimum resistance of the load equals the resistance of the coil during energy harvesting. However, this theory is inapplicable in electromagnetic vibration energy harvesters. This shortcoming of the application of the maximum transfer theory is due to its inability to consider the electrical damping effect (when current flows) on the mechanical behavior of the system (36). The analogous electrical value of the mechanical damping was thus included in calculating the optimal resistance value of the load. This method is more accurate. The value of the optimal resistance value of the load to maximize the harvested power output is defined in equation (7).

$$Rload, opt = Rcoil + \frac{K^2}{C} \quad (7)$$

The load voltage and power values are obtained from the numerical solution of equations (2) and (3). Thus, the load resistance voltage and its corresponding power output are expressed as in (8) and (9).

$$V(t) = K\dot{x}(t)\frac{Rload}{Rcoil+Rload} \quad (8)$$

$$P = \frac{V^2}{Rload} \quad (9)$$

2.4 Simulation of the different coil-magnet configurations

Four different configurations of the VEH were modeled and simulated. The *K* value of each configuration was calculated using equation (4). The obtained value in each model was then fed into the MATLAB Simulink model to obtain the values of the power generated from each harvester.

The load voltage (*V*) value can also be obtained from ANSYS Maxwell after simulations using the transient reports and rectangular plots. However, proper analysis can only be conducted on MATLAB using the polyfit function. From the plot of voltage generated versus time, the average value of the generated load voltage can be estimated. By combining these equations, the harvester's performance could be analyzed.

The ANSYS Maxwell models to test the effect of different geometrical configurations on the voltage and power generated in the EVEH are shown in Table 1. Four different structures of the EVEH were modeled using the software. The voltage and power generated from each of the models will be compared. The 2M1CFBS configuration represents a coil array, with two magnets repelling each other and a flat back shield. The repelling force provides more flux concentrations than the attracting forces (27, 37). The configuration 2M1CSBS is the same as the 2M1CFBS configuration except that it has a stepped-back shield. The H3M1CFBS configuration is a Halbach array that consists of three magnets, one coil, and a flat back shield. The two end magnets are arranged axially while the middle magnet is arranged radially according to their magnetic orientation from the north to the south pole. The H3M1CSBS configuration is the same as the H3M1CFBS configuration except that it has a stepped-back shield. The four configurations form different electromagnetic vibrational energy harvesters that will be examined and compared based on their outputs. The material used for the magnet is NdFeB N52 (neodymium iron boron) which has a coercive force of 977 KA/m and residual flux of 1.48 T while copper is used for the coil.

To validate the methodology for this research, the 2M1CFBS and the H3M1CFBS configurations which are reported as the best models for vibration energy harvesting as well as the design parameters were adopted from (12). The results of this study were compared with their work to observe any improvements. The main parts of the EVEH constitute the magnet inner, outer radius, and height, the coil inner, outer radius, and height, the back shield inner, outer radius, and height, the metallic elements inner, outer radius, and height as well as the coil-magnet, magnet-back shield air gaps and the mass of the moving magnet.

Table 1. Different experimental setups with their coil magnet configurations and additional metallic elements

Identity of model setup	Number of magnets	Number of coils	Type of back shield present
2M1CFBS	2	1	Flat
2M1CSBS	2	1	Stepped
H3M1CFBS	3	1	Flat
H3M1CSBS	3	1	Stepped

Table 2 shows the modified parameters and their dimensions. The volume of the stepped-back shield models, with dimensions carefully chosen based on design tolerances of at least 1mm, was added to the parameters.

Table 2. General parameters adopted for the EVEH design (12)

Parameters	
Magnets inner radius	2 mm
Magnets outer radius	12 mm
Magnets height	24 mm
Magnets material	NdFeB N52
Magnet coercive force	977 KA/m
Magnet residual flux	1.48 T
Coil inner radius (R_{in})	14 mm
Coil outer radius (R_{out})	16.5 mm
Coil height	12 cm
Coil material	Copper
Number of coil turns	2483
Resistance of coil	510 Ω
Coil fill factor	0.65
Back shield inner radius	18.5 mm
Back shield outer radius	20 mm
Back shield height	24 mm
Back shield material	1010 steel
Moving mass	0.792 Kg

Metallic element inner radius	14 mm
Metallic element outer radius	16.5 cm
Metallic element height	5.5 mm
Metallic element material	1010 steel
Excitation	10 Hz
Constraint volume of transducer (Flat back shield)	30.15 cm^3
Relative motion limit	4 mm

Source: Modified from Ordoñez, Robert (12)

Each of the four models was set up on the ANSYS Maxwell software and the magnets were set in motion in the band using motion setup tools from the ANSYS transient solver. A voltage is induced in the coil as the magnet oscillates (vibrates) relative to the coil. The schematic representation of each model setup is shown in Figure 5. The 3D section models are depicted on the right, while the 2D representations are on the left for better viewing and understanding.

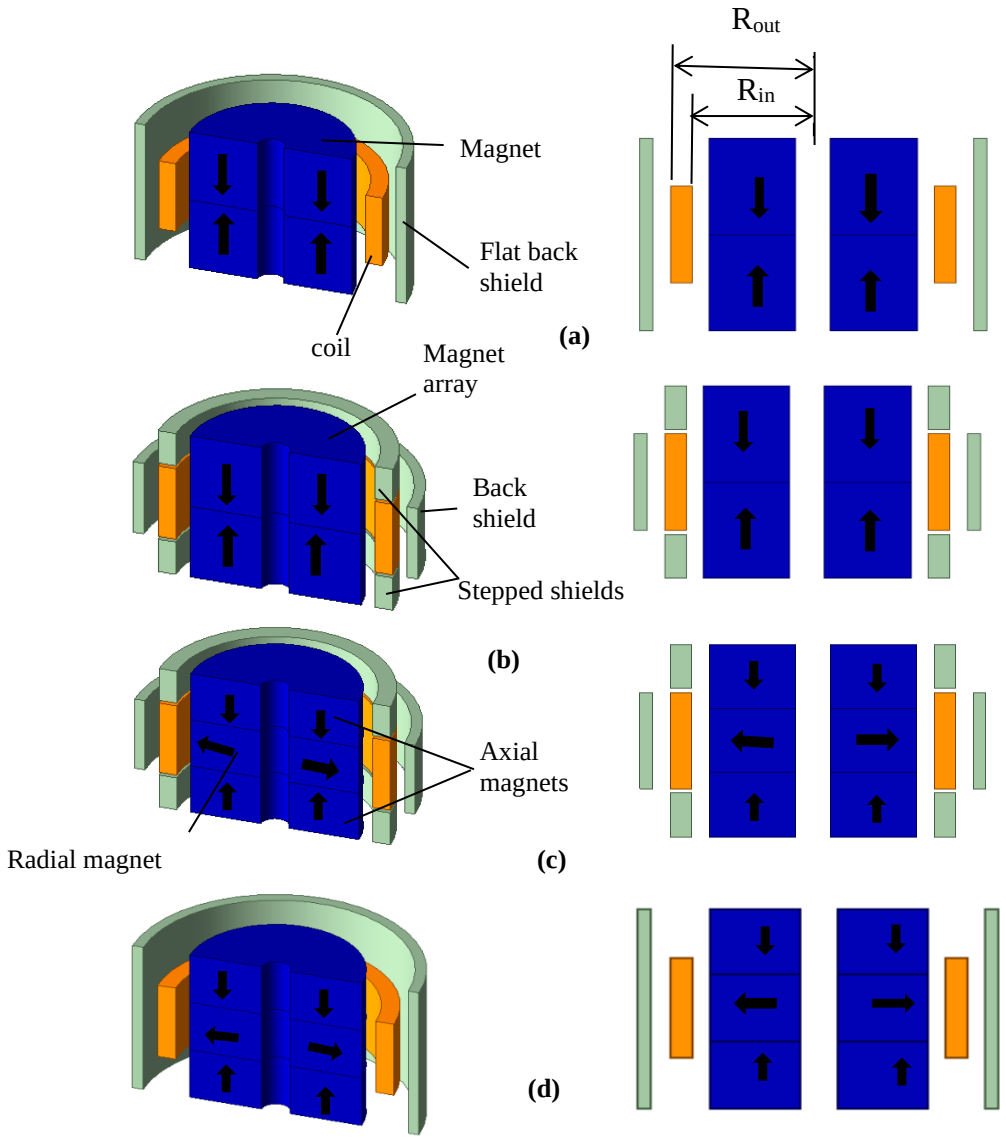

Figure 5. Different geometries of the EVEH showing the (a) 2M1CFBS, (b) 2M1CSBS, (c) H3M1CFBS, and the (d) H3M1CSBS configurations; 2D equivalents are shown on the left for easy visibility and understanding

The four models were each, connected to an external circuit that contains the load resistance and excited. The simulations were run using Maxwell axisymmetric 2D modelling which gives better meshing and more accurate results with less computer resources and time than 3D simulations.

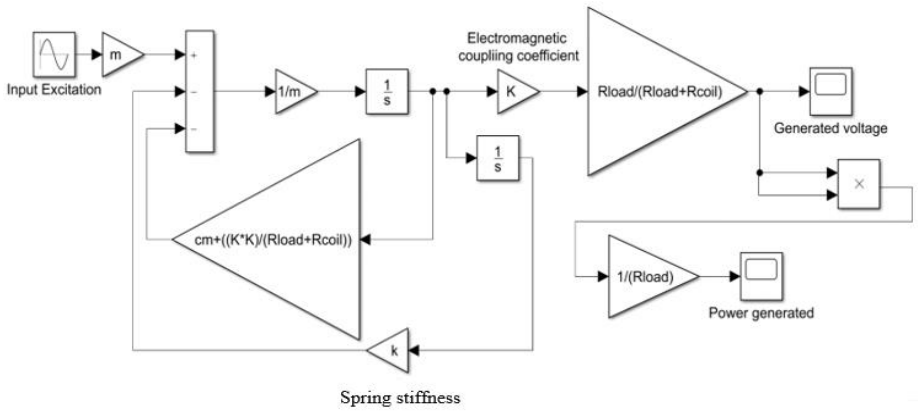

Figure 6. Numerical implementation of the model to obtain the power generated from the EVEH

The flux linkage and position data were then taken to MATLAB for post-analysis to calculate the value of *K*. Using the polynomial curve polyfit function, the flux change on the coil with the position of the moving mass (magnet) was computed. The value of the gradient of this curve obtained is the electromagnetic coupling coefficient *(K)* of the transducer. The variation of the power generated with vibrations was computed numerically using the MATLAB Simulink implemented model of equations (2), (3), and (9) shown in Figure 6.

The power density which is the power generated per unit volume of the EVEH will be calculated for each device using equation (10). This term is essential since adapting an energy harvesting device in an electric vehicle will require minimal volume and space constraints for the EVEH device.

$$PD = \frac{P}{V} \tag{10}$$

Where *PD* is the power density measured (W/cm^3), *P* is the power and V is the volume of the EVEH device.

3. RESULT AND DISCUSSION

Figure 7 shows the simulation results of the magnetic flux density from the 2D axisymmetric finite element analysis of each of the four models. The magnetic field lines and the magnetic flux density in brown and rainbow colors are shown on each model part (magnet, coil, back shield, and steps).

The variation in magnetic flux linkage on the coil for the four different configurations can be noticed.

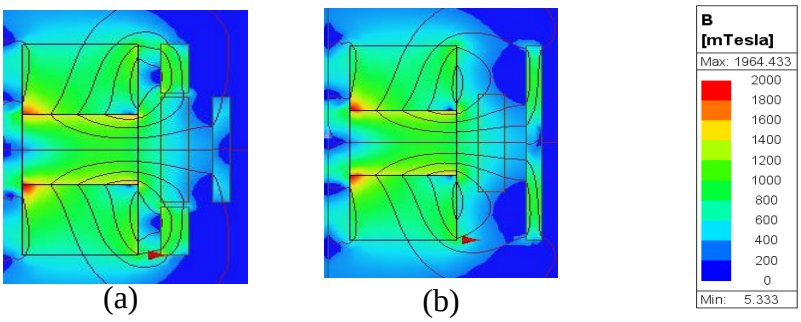

Figure 7. Axisymmetric 2D simulation results of (a) the H3M1CWME and (b) the H3M1C

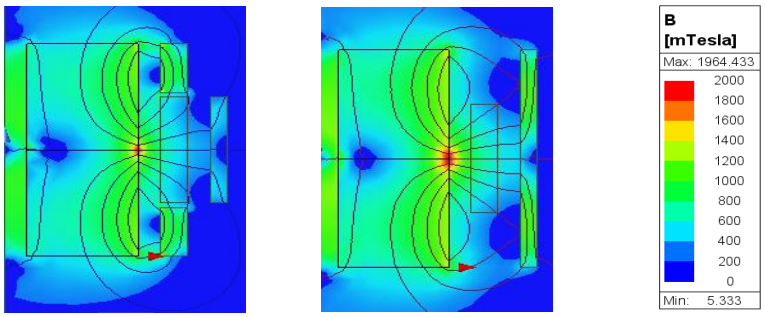

(c) (d)

Figure 7. Axisymmetric 2D simulation results of (c) the 2M1CWME and (d) the 2M1C configuration (continuation)

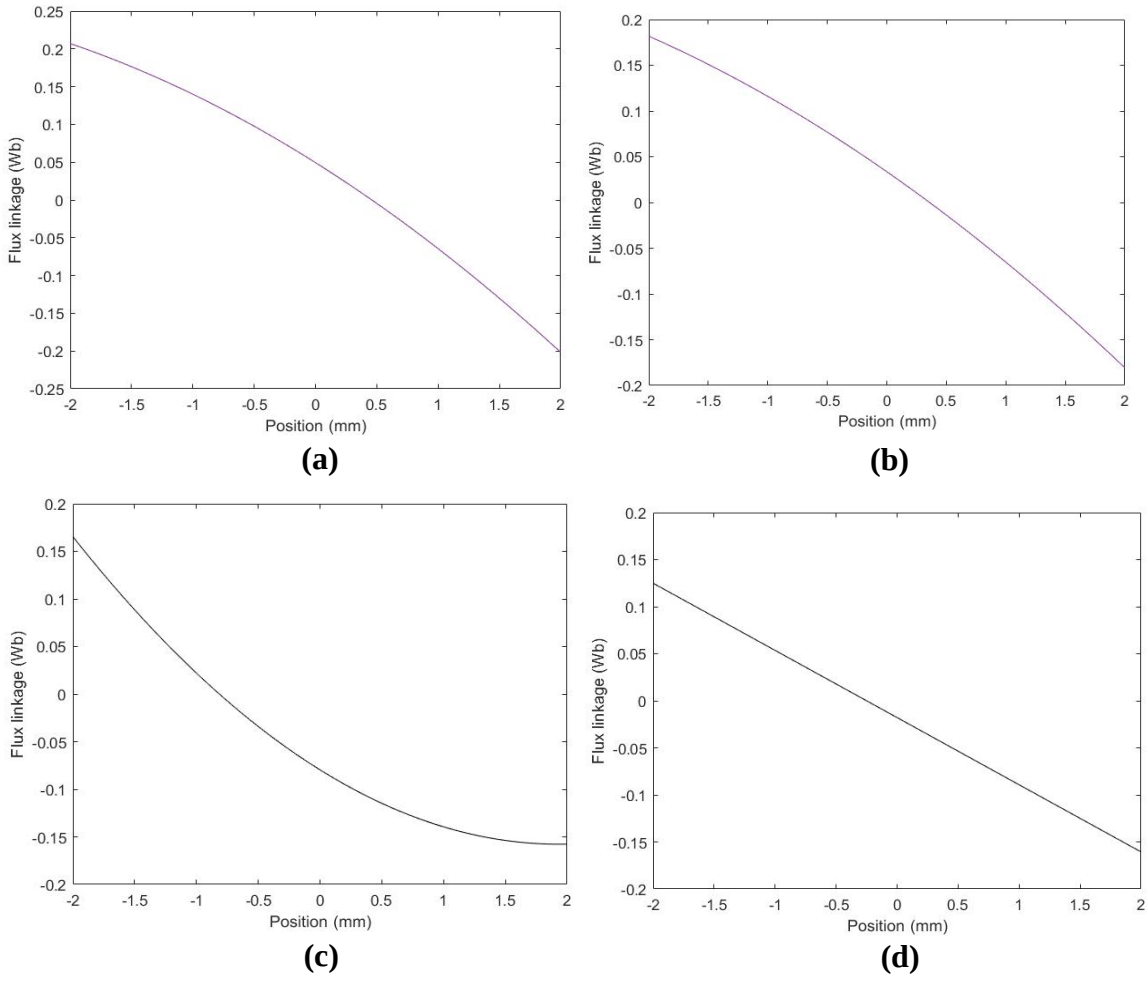

Figure 8. Plot of the magnetic flux linkage on the coil of the EVEH versus the position of the moving magnet arrays showing the (a) Halbach array with three magnets, one coil, and stepped back shield, (b) Halbach array with three magnets, one coil with flat back shield, (c) two magnets with one coil configuration with stepped back shield and (d) the two magnets with one coil configuration with flat back shield

Figure 8 shows the graphs of the flux linkage with the position of vibrating or moving mass (magnet) for each EVEH model. Figure 8(a) which is the Halbach array with three magnets and one coil with a stepped back shield (H3M1CSBS) is realized to produce a flux linkage of up to 0.22 Wb at the position -2 mm. Meanwhile, the same configuration with a

flat back shield (H3M1CFBS) in Figure 8(b) produces a maximum flux linkage of 0.19 Wb at the same position of -2 mm. Likewise, the configuration with two magnets, one coil, and a stepped back shield (2M1CSBS) in Figure 8(c) is observed to produce a flux linkage of up to 0.17 Wb at the position -2 mm. Meanwhile, the configuration in Figure 8(d) with a flat back shield produces 0.14 Wb of flux linkage at that same position.

Table 3 compares the results obtained from this study and those from (12) in terms of flux linkage. The models used to compare with their work are the H3M1CFBS and the 2M1CFBS configurations since they are similar in structure.

Table 3. Comparison of the results obtained from this study and previous studies for validation of methodology

Configuration	**Flux linkage (Wb)**	
	Our study	Ordoñez, Robert (12)
H3M1CFBS (at -2 mm)	0.19	0.2
2M1CFBS (at -2 mm)	0.14	0.18

The values in Table 3 show close similarity. This shows the validity of the methodology used in this study. The minimal difference may be due to the use of different software.

The maximum instantaneous voltages generated from each of the models and their corresponding electromagnetic coupling coefficients *(K)* are shown in Table 4.

The Halbach array is seen to produce more energy than the non-Halbach arrays. The configurations with a stepped-back shield are seen to perform better than those with flat-back shields. A difference of at least 7 V is observed in the generated voltage between the configurations with stepped-back shields and those with stepped-back shields. The increase in voltage generation in the configurations with stepped-back shields is due to an increase in flux linkage to their coils. This increase in flux linkage is due to the reduction of the air gap between the magnet and the back shield. A reduced air gap leads to a reduction of the magnetic reluctance to the flux linkage which then increases the amount of linkage flux to the coils. The air gap between the back shield and the magnet in the configurations with flat back shields (the 2M1CFBS and H3M1CFBS configurations) is more than the air gap in the configurations with stepped back shields (the 2M1CSBS and H3M1CSBS). The modification has concentrated the flux more on the coils, it leads to more power generation.

Table 4. Maximum flux linkage, electromagnetic coupling coefficient values (K), and corresponding generated voltages of different magnet-coil configurations

Configuration	**Maximum flux linkage (Wb)**	**Electromagnetic coupling coefficient (Wb/m)**	**Maximum generated voltage (V)**	**Power generated (W)**	**Total volume (cm^3)**
H3M1CSBS	0.22	110	36.00	2.54	19.77
H3M1CFBS	0.19	95	23.75	1.11	30.15
2M1CSBS	0.17	85	27.40	1.47	19.77
2M1CFBS	0.14	70	20.00	0.78	30.15

Comparing the configurations, it is realized that more power is generated per unit volume (19.77 cm^3) in the geometries with stepped-back shields compared to a volume of 30.15 cm^3 in the flat-back shields. The Halbach array with one coil, three magnets, and a stepped-back shield array has generated a power density of 0.13 W/cm^3, calculated using equation (10).

4. CONCLUSION

The configurations with stepped-back shield geometries produced more flux linkage, induced voltage, transduction factor, and power with less device volume compared to the configurations with flat-back shields. However, the Halbach array with three magnets and one coil with a stepped back shield (H3M1CSBS) produced the highest amount of flux linkage, transduction factor, induced voltage, and generated power compared to other configurations under the same excitation conditions. Thus, it is the recommended

configuration for harvesting vibrational energy in electric vehicles for application in agricultural transportation. Less volume was also taken by the device compared to devices from previous studies. Volume is a very important constraint in energy harvesting devices since they must fit into very tiny available spaces in the electric vehicle transmission system.

H3M1CSBS configuration is considered to be optimized using an artificial intelligence-based algorithm to produce the best value of harvested energy using minor resources such as coil diameter, height, and magnet sizes. The optimized model should be realized and adapted to a real-world agricultural transportation electric tricycle and tested for performance.

ACKNOWLEDGMENTS

None

CONFLICT OF INTEREST

None

REFERENCES

1. Gao T, Erokhin V, Arskiy A. Dynamic Optimization of Fuel and Logistics Costs as a Tool in Pursuing Economic Sustainability of a Farm. Sustainability. 2019;11:5463. doi: https://doi.org/10.3390/su11195463
2. Savić B, Mladen P, Zorica V. The Impact Of Transportation Costs On Economic Performances In Crop Production. Economics of Agriculture. 2020;67(3):683-97. doi: 10.5937/ekoPolj2003683S
3. Brian B, Shahe ME, Shilpi F, Xu L. Transport Costs, Comparative Advantage, and Agricultural Development: Evidence from Jamuna Bridge in Bangladesh. SSRN Electronic Journal. 2018. doi: http://dx.doi.org/10.2139/ssrn.3176160
4. Siang FT, Chee WT. A review of energy sources and energy management system in electric vehicles. Renewable and Sustainable Energy Reviews, Elsevier. 2013;20:82-102. doi: https://doi.org/10.1016/j.rser.2012.11.077
5. Sonali GA, Renu SA, Akshay KRB. A review on barrier and challenges of electric vehicle in India and vehicle to grid optimization. Transportation Engineering Elsevier Ltd. 2021;4:1-10. doi: https://doi.org/10.1016/j.treng.2021.100057
6. Ntombela M, Kabeya M, Katleho M. A Comprehensive Review for Battery Electric Vehicles (BEV) Drive Circuits Technology, Operations, and Challenges. World Electric Vehicle Journal. 2023;14(7):1-23. doi: https://doi.org/10.3390/wevj14070195
7. Caban J, Vrabel J, Górnicka D, Nowak R, Jankiewicz M, Matijošius J, Palka M. Overview of Energy Harvesting Technologies used in Road Vehicles. Energies. 2023;16(3787):1-32. doi: https://doi.org/10.3390/en16093787
8. Briand D, Yeatman E, Roundy S. Micro Energy Harvesting. 2015. 1-468 p.
9. Spreemann D, Manoli Y. Electromagnetic Vibration Energy Harvesting Devices: Architectures, Design, Modeling and Optimization. 1 ed. Berlin/Heidelberg, Germany: Springer Dordrecht; 2012. 198 p. doi: https://doi.org/10.1007/978-94-007-2944-5
10. Zhu D, Beeby S, Tudor J, Harris N. Increasing output power of electromagnetic vibration energy harvesters using improved Halbach arrays. Sens Actuator A Phys. 2013(203):11–9. doi: https://doi.org/10.1016/j.sna.2013.08.008
11. Li Z, Yan Z, Luo J, Yang Z. Performance comparison of electromagnetic energy harvesters based on magnet arrays of alternating polarity and configuration. Energy Convers Manag. 2019;179:132–40. doi: https://doi.org/10.1016/j.enconman.2018.10.060
12. Ordoñez V, Robert A, Jordi R, Salvatore R. Analysis of different cylindrical magnet and coil configurations for electromagnetic vibration energy harvesters. Periodicals of Engineering and Natural Sciences 2021;9(2):1055-63. doi: 10.21533/pen.v9i2.2044
13. Phan TN, Jesus JA, Bengt O, Sebastian B. Design Optimization and Comparison of Cylindrical Electromagnetic Vibration Energy Harvesters. Sensors. 2021;21:1-18. doi: https://doi.org/10.3390/s21237985

14. Lopez DP, Gabilondo I, Alarcon E, Moll F, . Mechanical energy harvesting taxonomy for industrial environments: Application to the railway industry. IEEE Transactions on Intelligent Transportation Systems. 2020;21:2696–706. doi: 10.1109/TITS.2019.2924987
15. Uchino K. Piezoelectric energy harvesting Systems—Essentials to Successful Developments. Energy Technology 2018;6:829–48. doi: https://doi.org/10.1002/ente.201700785
16. Davidson J, Mo C. Recent advances in energy harvesting technologies for structural health monitoring applications. Smart Materials Research. 2014;2014(1):14. doi: https://doi.org/10.1155/2014/410316
17. Saha CR. Modelling theory and applications of the electromagnetic vibrational generator: Elsivier; 2011. doi: 10.5772/27236
18. Guo X, Zhang Y, Fan K, Lee C, Wang F. A comprehensive study of non linear air damping and "pull-in" effects on the electrostatic energy harvesters. Energy Conversion and Management. 2020;203:112264. doi: https://doi.org/10.1016/j.enconman.2019.112264
19. Beeby S, Kazmierski TJ. Energy harvesting systems: Principles, modeling and applications,. 1 ed. New York, NY: Springer; 2011. 163 p. doi: https://doi.org/10.1007/978-1-4419-7566-9
20. Rahimi A, Zorlu O, Muhtaroglu A, Kulah H. Fully self-powered electromagnetic energy harvesting system with highly efficient dual rail output. IEEE Sensors Journal 2012;12(6):2287–98. doi: 10.1109/JSEN.2011.2177967
21. Liu H, Xia Y, Chen T, Yang Z, Liu W, Wang P, Sun L. Study of a hybrid generator based on triboelectric and electromagnetic mechanisms. IEEE Sensors Journal. 2017;17:3853–60. doi: 10.1109/JSEN.2017.2694458
22. El-Rayes K, Gabran S, Abdel-Rahman E, Melek W. Variable-flux biaxial vibration energy harvester. IEEE Sensors Journal 2018;18(8):3218–27. doi: 10.1109/JSEN.2018.2805287
23. Park H, Kim J. Electromagnetic induction energy harvester for high-speed railroad applications. International Journal of Precision Engineering and Manufacturing- Green Technology. 2016;3:41–8. doi: https://doi.org/10.1007/s40684-016-0006-6
24. Vocca H, Cottone F. Kinetic energy harvesting: IntechOpen; 2014. doi: 10.1007/978-1-4419-7566-9_1
25. Wang X. Frequency analysis of vibration energy harvesting systems: Academic Press; 2016.
26. Williams C, Shearwood C, Harradine M, Mellor P, Birch T, Yates R. Development of an electromagnetic micro-generator. IEE Proceedings: Circuits, Devices and Systems. 2001;148(5):337–42. doi: 10.1049/ip-cds:20010525
27. Shahosseini I, Najafi K. Cylindrical Halbach magnet array for electromagnetic vibration energy harvesters. In: 28, editor. IEEE International Conference on Micro Electro Mechanical Systems2015. p. 1051-4. doi: 10.1109/MEMSYS.2015.7051143
28. Zhu D, Beeby S, Tudor J, Harris N. Vibration energy harvesting using the Halbach array. Smart Materials and Structures. 2012;21(7):075020. doi: doi:10.1088/0964-1726/21/7/075020
29. Bjørk R, Bahl CR, Smith A, Pryds N. Comparison of adjustable permanent magnetic field sources. Journal of Magnetism and Magnetic Materials. 2010;322(22):3664–71. doi: https://doi.org/10.1016/j.jmmm.2010.07.022
30. Eka BS, Ahmad Z, Andriansyah, Wahyu BS. Analysis Static of Chassis Robot Arm as Design Modification Induction Melting Furnace Machine using FEA Method. Journal of Renewable Energy & Mechanics (REM) 2023;6(2):86-98. doi: https://doi.org/10.25299/rem.2023.14344
31. Meeker JDC. Finite Element Method Magnetics, ver. 4.22015 October 25, 2015.
32. Baltzis K. The finite element method magnetics (FEMM) freeware package: May it serve as an educational tool in teaching electromagnetics? Education and Information Technologies. 2010;15:19-36. doi: https://doi.org/10.1007/s10639-008-9082-8
33. Spreemann D, Homann D, Folkmer B, Manoli Y. Numerical optimization approach for resonant electromagnetic vibration transducer designed for random vibration. JMicromech Microeng. 2008;18:104001. doi: 10.1088/0960-1317/18/10/104001
34. Rao SS. Mechanical Vibrations. 5th ed. Chennai, India: Pearson; 2011.

35. Mario M, Gerhard F. A Comparison of Methods to Measure the Coupling Coeffcient of Electromagnetic Vibration Energy Harvesters. Micromachines 2019;10(826):1-14. doi: https://doi.org/10.3390/mi10120826
36. Stephen NG. On energy harvesting from ambient vibration. Journal of Sound and Vibration. 2006;293:409–25. doi: https://doi.org/10.1016/j.jsv.2005.10.003
37. Yaşar O, Uluşan H, Zorlu Ö, Şardan-Sukas Ö, Külah H. Optimization of AA-battery sized electromagnetic energy harvesters: Reducing the resonance frequency using a non-magnetic inertial mass. IEEE Sensors Journal. 2018;18(11):4509-16. doi: 10.1109/JSEN.2018.2819194